

Resonant sneutrino production in Supersymmetry with R-parity violation at the LHC

G. Moreau

*Service de Physique Théorique
CEA-Saclay, F91191, Gif-sur-Yvette, Cedex France*

E. Perez

*Service de Physique des Particules, DAPNIA
CEA-Saclay, F91191, Gif-sur-Yvette, Cedex France*

G. Polesello

INFN, Sezione di Pavia, Via Bassi 6, Pavia, Italy

Abstract

The resonant production of sneutrinos at the LHC via the R-parity violating couplings $\lambda'_{ijk} L_i Q_j D_k^c$ is studied through its three-leptons signature. A detailed particle level study of signal and background is performed using a fast simulation of the ATLAS detector. Through the full reconstruction of the cascade decay, a model-independent and precise measurement of the masses of the involved sparticles can be performed. Besides, this signature can be detected for a broad class of supersymmetric models, and for a wide range of values of several λ'_{ijk} coupling constants. Within the MSSM, the production of a 900 GeV sneutrino for $\lambda'_{211} > 0.05$, and of a 350 GeV sneutrino for $\lambda'_{211} > 0.01$ can be observed within the first three years of LHC running.

1 Introduction

The most general superpotential respecting the gauge symmetries of the Standard Model (SM) contains bilinear and trilinear terms which are not taken into account in the Minimal Supersymmetric Standard Model (MSSM). Restricting to the trilinear part, these additional terms read as :

$$W \supset \sum_{i,j,k} \left(\frac{1}{2} \lambda_{ijk} L_i L_j E_k^c + \lambda'_{ijk} L_i Q_j D_k^c + \frac{1}{2} \lambda''_{ijk} U_i^c D_j^c D_k^c \right), \quad (1)$$

where i, j, k are generation indices, L (Q) denote the left-handed leptons (quarks) superfields, and E^c , D^c and U^c are right-handed superfields for charged leptons, down and up-type quarks, respectively.

The first two terms in Eq.(1) lead to violation of the lepton number (\not{L}), while the last one implies violation of the baryon number (\not{B}). Since the simultaneous presence of \not{L} and \not{B} couplings could lead to a too fast proton decay, a discrete multiplicative symmetry which forbids the above terms in the superpotential has been imposed by hand in the MSSM. This symmetry, called R-parity (R_p), is defined as $R_p = (-1)^{3B+L+2S}$, where B , L and S respectively denote the baryon number, the fermion number and the spin, such that $R_p = -1$ ($R_p = 1$) for all supersymmetric (SM) particles. However other solutions can ensure the proton stability, e.g. if L only is violated, or if only $U_i^c D_j^c D_k^c$ interactions are allowed and the proton is lighter than the Lightest Supersymmetric Particle (LSP). Moreover, on the theoretical point of view, there is no clear preference, e.g. in models inspired by Grand Unified or string theories, between \not{R}_p and R_p conservation [1]. It is thus mandatory to search for SUSY in both scenarios.

On the experimental side, the main consequence of \not{R}_p lies in the possibility for the LSP to decay into ordinary matter. This is in contrast to scenarios where R_p is conserved, in which the LSP is stable and escapes detection, leading to the characteristic search for missing energy signals in direct collider searches. Moreover, while in R_p conserved models, the supersymmetric (SUSY) particles must be produced in pairs, \not{R}_p allows the single production of superpartners, thus enlarging the mass domain where SUSY could be discovered. In particular, \not{R}_p couplings offer the opportunity to resonantly produce supersymmetric particles [2, 3]. Although the \not{R}_p coupling constants are severely constrained by the low-energy experimental bounds [1, 4, 5, 6, 7, 8], the superpartner resonant production can have significant cross-sections both at leptonic [4] and hadronic [9] colliders. This is this possibility which is exploited throughout this paper.

The resonant production of supersymmetric particles is attractive for another reason: Since its rate is proportional to a power 2 of the relevant \not{R}_p coupling, this reaction would allow an easier determination of the \not{R}_p couplings than the

pair production. In fact in the latter case, the sensitivity on the \mathcal{R}_p coupling is mainly provided by the displaced vertex analysis for the LSP decay, which is difficult experimentally especially at hadronic colliders.

In this paper, we focus on the resonant SUSY particle production at the Large Hadron Collider (LHC) operating at a center of mass energy of 14 TeV with special reference to the ATLAS detector. At the LHC due to the continuous distribution of the centre of mass energy of the colliding partons, a parton-parton resonance can be probed over a wide mass domain. This is a distinct advantage over the situation at lepton colliders, where the search for narrow resonances requires lengthy scans over the centre of mass energy of the machine.

At hadronic colliders, either a slepton or a squark can be produced at the resonance through a λ' or a λ'' coupling constant, respectively. In the hypothesis of a single dominant \mathcal{R}_p coupling constant, the resonant SUSY particle could decay through the same \mathcal{R}_p coupling as in the production, leading then to a two quarks final state for the hard process [10, 11, 12, 13, 14]. In the case where both λ' and λ couplings are non-vanishing, the slepton produced via λ' can decay through λ giving rise to the same final state as in Drell-Yan process, namely two leptons [13, 15, 16, 17]. However, for most of the values of the \mathcal{R}_p coupling constants allowed by present indirect searches, the decays of the resonant SUSY particle via gauge interactions are dominant if kinematically accessible [4]. In this favoured situation, typically, the produced superpartner initiates a cascade decay ended by the \mathcal{R}_p decay of the LSP. In case of a dominant λ'' coupling constant, due to the \mathcal{R}_p decay of the LSP into quarks, this cascade decay leads to multijet final states which have a large QCD background [9, 10]. Only if leptonic decays such as for instance $\tilde{\chi}_1^+ \rightarrow \bar{l}_i \nu_i \tilde{\chi}_1^0$ enter the cascade clearer signatures can be investigated [18]. The situation is more favourable in the hypothesis of a single λ' coupling constant, where the LSP can decay into a charged lepton, allowing then multileptonic final states to be easily obtained.

We will thus assume a dominant λ'_{ijk} coupling constant. At hadronic colliders, either a $\tilde{\nu}_i$ sneutrino or a \tilde{l}_i charged slepton can be produced at the resonance via λ'_{ijk} and the initial states are $d_j \bar{d}_k$ and $u_j \bar{d}_k$, respectively. The slepton produced at the resonance has two possible gauge decays, either into a chargino or a neutralino. In both cases particularly clean signatures can be observed. For example, the production of a neutralino together with a charged lepton resulting from the resonant charged slepton production can lead to the interesting like-sign dilepton topology [19, 20] since, due to its Majorana nature, the neutralino decays via λ'_{ijk} into a lepton as $\tilde{\chi}^0 \rightarrow l_i u_j \bar{d}_k$ and into an anti-lepton as $\tilde{\chi}^0 \rightarrow \bar{l}_i \bar{u}_j d_k$ with the same probability.

In this article, we consider the single lightest chargino production at LHC as induced by the resonant sneutrino production $pp \rightarrow \tilde{\nu}_i \rightarrow \tilde{\chi}_1^\pm l_i$. The single $\tilde{\chi}_1^\pm$

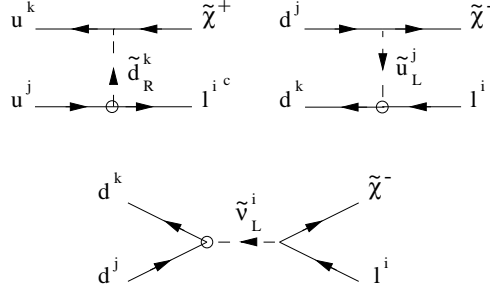


Figure 1: *Feynman diagrams for the single chargino production at hadronic colliders via the λ'_{ijk} coupling (symbolised by a circle in the figure). The arrows denote the flow of the particle momentum.*

production also receives contributions from the t and u channel squark exchange diagrams shown in Figure 1. In many models, the $\tilde{\chi}_1^0$ neutralino is the LSP for most of the SUSY parameter space. In the hypothesis of a $\tilde{\chi}_1^0$ LSP, the produced $\tilde{\chi}_1^\pm$ chargino mainly decays into the neutralino as $\tilde{\chi}_1^\pm \rightarrow \tilde{\chi}_1^0 q_p \bar{q}'_p$ or as $\tilde{\chi}_1^\pm \rightarrow \tilde{\chi}_1^0 l_p^\pm \nu_p$. The neutralino then decays via λ'_{ijk} as $\tilde{\chi}_1^0 \rightarrow l_i u_j \bar{d}_k$, $\bar{l}_i \bar{u}_j d_k$ or as $\tilde{\chi}_1^0 \rightarrow \nu_i d_j \bar{d}_k$, $\bar{\nu}_i \bar{d}_j d_k$. We concentrate on the decays of both the chargino and the neutralino into charged leptons, which lead to a three leptons final state. This signature has a low Standard Model background, and allows the reconstruction of the whole decay chain, thus providing a measurement of some parameters of the SUSY model.

2 The signal

2.1 Theoretical framework

Our theoretical framework in sections 2 and 3 will be the \mathcal{R}_p extension of the Minimal Supersymmetric Standard Model. In Section 4 we will also give results in the Minimal Supergravity (mSUGRA) model. The MSSM parameters are the following. M_1 , M_2 and M_3 are the soft-SUSY breaking mass terms for the bino, the wino and the gluino, respectively. μ is the Higgs mass parameter. $\tan\beta = \langle H_u \rangle / \langle H_d \rangle$ is the ratio of the vacuum expectation values (vev) for the two-Higgs doublet fields. A_t , A_b and A_τ are the third generation soft-SUSY breaking trilinear couplings. In fact, since these trilinear couplings are proportional to the fermion masses one can neglect the first two generations couplings without any phenomenological consequence in this context. Finally, $m_{\tilde{q}}$, $m_{\tilde{l}}$ and $m_{\tilde{\nu}}$ are the squark, slepton and sneutrino mass, respectively. The value of the squark mass enters our study mainly in the determination of the

relative branching ratios of the $\tilde{\chi}^0$ into lepton or neutrino and of the $\tilde{\chi}^\pm$ into $\tilde{\chi}^0$ + quarks or $\tilde{\chi}^0$ + leptons. The remaining three parameters $m_{H_u}^2$, $m_{H_d}^2$ and the soft-SUSY breaking bilinear coupling B are determined through the electroweak symmetry breaking conditions which are two necessary minimisation conditions of the Higgs potential.

We choose to study the case of a single dominant λ'_{2jk} allowing the reactions $pp \rightarrow \tilde{\chi}^\pm \mu^\mp$. In section 3 the analysis will be performed explicitly for the λ'_{211} coupling, since it corresponds to the hard subprocess $d\bar{d} \rightarrow \tilde{\chi}_1^\pm \mu^\mp$ which offers the highest partonic luminosity. We will take $\lambda'_{211}=0.09$, the upper value allowed by indirect bound: $\lambda'_{211} < 0.09(m_{\tilde{d}_R}/100\text{GeV})$ [1] for a squark mass of 100 GeV. A quantitative discussion will be given below for the general case of a single dominant λ'_{2jk} coupling constant. We will not treat explicitly the λ'_{1jk} couplings which are associated to the $\tilde{\chi}^\pm e^\mp$ production, since the low-energy bounds on these couplings are rather more stringent than the constraints on λ'_{2jk} and λ'_{3jk} [1]. However, the three-leptons analysis from sneutrino production should give similar sensitivities on the λ'_{1jk} and λ'_{2jk} couplings since isolation cuts will be included in the selection criteria for the leptons. We will not perform the analysis of the λ'_{3jk} couplings which correspond to the $\tilde{\chi}^\pm \tau^\mp$ production. A technique for mass reconstruction in the ATLAS detector using the hadronic decays of the τ has been demonstrated in [21]. The detailed experimental analysis needed to extract a signal is beyond the scope of this work. Besides, in this case the sneutrino and chargino mass reconstruction studied in Section 3.1 is spoiled by the neutrinos produced in the τ decay.

2.2 Single chargino production cross-section

In order to establish the set of models in which the analysis presented below can be performed, we need to study the variations of the single chargino production rate $\sigma(pp \rightarrow \tilde{\chi}^\pm \mu^\mp)$ with the MSSM parameters.

In Figure 2, we present the cross-sections for the $\tilde{\chi}_1^\pm \mu^\mp$ production through several λ'_{2jk} couplings as a function of the μ parameter for the fixed values: $\tan\beta=1.5$, $M_2 = 200$ GeV, and $m_{\tilde{\nu}} = 400$ GeV. For this choice of parameters and independently of μ , the chargino $\tilde{\chi}_1^\pm$ is lighter than the $\tilde{\nu}$. In this case the contributions of squark exchange in the t and u channels are negligible compared to the resonant process so that the $\tilde{\chi}_1^\pm \mu^\mp$ production cross-section does not depend on the squark mass. The values for the considered \mathcal{R}_p coupling constants have been conservatively taken equal to the low-energy limits for a sfermion mass of 100 GeV [1]. The cross-sections scale as λ_{2jk}^2 .

We see on this Figure that the dependence of the rates on μ is smooth for $|\mu| > M_2$. This is due to the weak dependence of the $\tilde{\chi}_1^\pm$ mass on μ in this do-

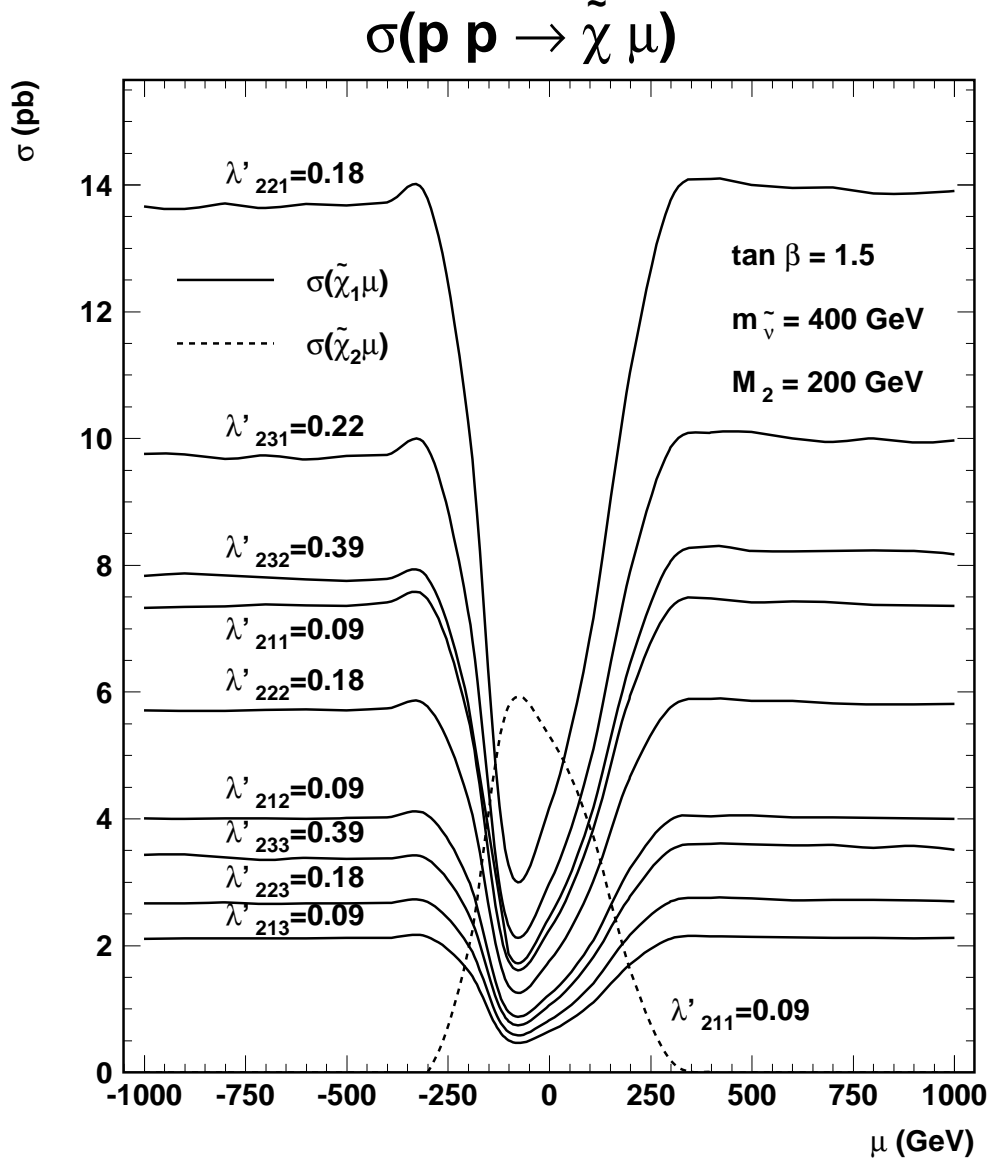


Figure 2: Cross-sections for the $\tilde{\chi}_1^\pm - \mu^\mp$ production as a function of the μ parameter through various λ'_{2jk} couplings, for $\tan \beta = 1.5$, $M_2 = 200$ GeV and $m_{\tilde{\nu}} = 400$ GeV. In the case of λ'_{211} the cross-section for $\tilde{\chi}_2^\pm - \mu^\mp$ is also shown as the dashed line. The values of the \mathcal{R}_p couplings have been chosen equal to: $\lambda'_{211} = 0.09$, $\lambda'_{212} = 0.09$, $\lambda'_{213} = 0.09$, $\lambda'_{221} = 0.18$, $\lambda'_{222} = 0.18$, $\lambda'_{223} = 0.18$, $\lambda'_{231} = 0.22$, $\lambda'_{232} = 0.39$ and $\lambda'_{233} = 0.39$, which correspond to the low-energy limits for a sfermion mass of 100 GeV [1].

main. In contrast, we observe a strong decrease of the rate in the region $|\mu| < M_2$ where the $\tilde{\chi}_1^\pm$ chargino is mainly composed by the higgsino. Most of the small $|\mu|$ domain ($|\mu|$ smaller than ~ 100 GeV for $\tan\beta = 1.41$ and $m_0 = 500$ GeV) is however excluded by the present LEP limits [30].

We also show as a dashed line on the plot the rate for the $\tilde{\chi}_2^\pm\text{-}\mu^\mp$ production through the λ'_{211} coupling. The decrease of the $\tilde{\chi}_2^\pm$ production rate with increasing $|\mu|$ is due to an increase of the $\tilde{\chi}_2^\pm$ mass. We will not consider the contribution to the three-leptons final state from the $\tilde{\chi}_2^\pm$ production since the rate becomes important only for a very limited range of small $|\mu|$ values not yet excluded by LEP data.

Figure 2 also allows to compare the sensitivities that can be reached on various λ'_{2jk} couplings using the single chargino production. If we compare for instance the cross-sections of the $\tilde{\chi}_1^\pm$ production via λ'_{211} and λ'_{221} at $\mu = -500$ GeV, we can see that for equal values of the R_p couplings the ratios between the cross-sections associated to λ'_{211} and λ'_{221} is ~ 2.17 . Therefore, the sensitivity that can be obtained on λ'_{221} is only $\sim \sqrt{2.17}$ times weaker than the sensitivity on λ'_{211} , for a 400 GeV sneutrino. Note that the cross-section ratio, and hence the scaling to be applied, in order to infer from the reach on λ'_{211} the sensitivity on another coupling λ'_{2jk} , depends on the sneutrino mass. The reason is that the evolution of the parton densities with the x -Bjorken variable is different for sea quark and valence quark and for different quark flavours.

In order to study the dependence of the cross-section on the masses of the involved sparticles, the parameters $m_{\tilde{\nu}}$ and M_2 were varied, and the other model parameters affecting the cross-section were fixed at the values: $\lambda'_{211} = 0.09$, $\mu = -500$ GeV and $\tan\beta = 1.5$. The cross-section for $\tilde{\chi}_1^\pm\text{-}\mu^\mp$ production as a function of $m_{\tilde{\nu}}$ and $m_{\tilde{\chi}_1^\pm}$ is shown in Figure 3. Since the $\tilde{\chi}_1^\pm$ mass is approximately equal to M_2 as long as $M_2 < |\mu|$, and becomes equal to $|\mu|$ for $M_2 > |\mu|$, we studied $\tilde{\nu}$ masses between 100 and 950 GeV, and values of M_2 between 100 and 500 GeV. For increasing $m_{\tilde{\nu}}$ the cross-section decreases due to a reduction of the partonic luminosity. A decrease of the cross-section is also observed for $m_{\tilde{\chi}_1^\pm}$ approaching $m_{\tilde{\nu}}$, since the phase space factor of the decay $\tilde{\nu} \rightarrow \tilde{\chi}_1^\pm \mu^\mp$ following the resonant sneutrino production is then suppressed. In the region $m_{\tilde{\chi}_1^\pm} > m_{\tilde{\nu}}$, the chargino production still receives contributions from the s channel exchange of a virtual sneutrino, as well as from the t and u channels squark exchange which in that case also contribute significantly. However, in this phase space domain where the resonant sneutrino production is not accessible, the cross-section is considerably reduced.

Finally, the single chargino production rate depends weakly on the A trilinear couplings. Indeed, only the t and u channels squark exchange, varying with the squark mass which can be influenced by A , depends on these couplings. The

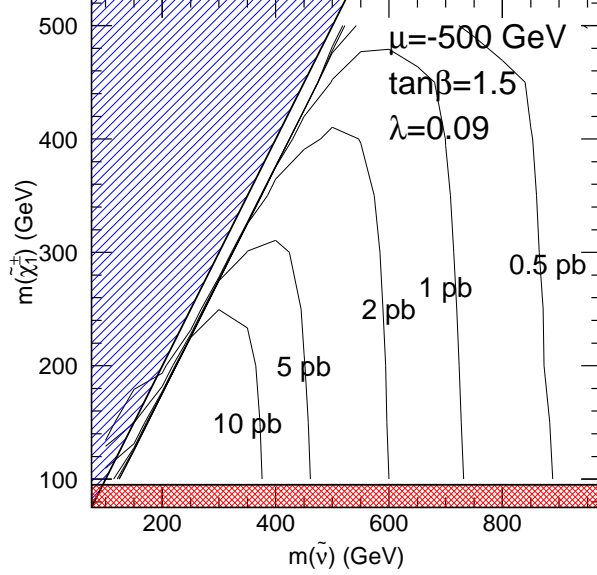


Figure 3: Cross-section for $\tilde{\chi}_1^\pm - \mu^\mp$ production as a function of $m_{\tilde{\nu}}$ and $m_{\tilde{\chi}_1^\pm}$ in the MSSM for the choice of values $\mu = -500$ GeV, $\tan\beta = 1.5$ and $\lambda'_{211} = 0.09$. The hatched region at the upper left corresponds to $m_{\tilde{\nu}} < m_{\tilde{\chi}_1^\pm}$. The cross-hatched region at low $m_{\tilde{\chi}_1^\pm}$ is excluded by the preliminary LEP results at $\sqrt{s} = 196$ GeV [30].

dependence of the rate on the $\tan\beta$ parameter is also weak.

2.3 Three leptons branching ratio

We calculate the total three leptons rate by multiplying the single chargino cross-section by the chargino branching ratio, since we neglect the width of the chargino. The three-leptons final state is generated by the cascade decay $\tilde{\chi}_1^\pm \rightarrow \tilde{\chi}_1^0 l_p^\pm \nu_p$, $\tilde{\chi}_1^0 \rightarrow \mu u d$. For $m_{\tilde{\nu}}, m_{\tilde{l}}, m_{\tilde{q}}, m_{\tilde{\chi}_2^0} > m_{\tilde{\chi}_1^\pm}$, the chargino decays mainly into a real or virtual W and a $\tilde{\chi}_1^0$ and hence its branching fraction for the decay into leptons (lepton = e, μ) is $\sim 22\%$. In particular kinematic configurations, the R_p modes can compete with the gauge couplings, affecting the $\tilde{\chi}_1^\pm$ branching fractions. However, this does not happen as long as the chargino is sufficiently heavier than the neutralino, as is the case for example in supergravity inspired models. When $\tilde{\chi}_1^0$ is the LSP, the branching ratio $B(\tilde{\chi}_1^0 \rightarrow \mu u d)$ ranges between $\sim 40\%$ and $\sim 70\%$. For values of $|\mu|$ much smaller than M_2 the other allowed

decay $\tilde{\chi}_1^0 \rightarrow \nu_\mu dd$ becomes dominant, spoiling the three-leptons signature.

3 Experimental analysis

3.1 Mass reconstruction

The analysis strategy is based on the exploitation of the decay chain:

$$\begin{array}{lcl} \tilde{\nu}_\mu & \rightarrow & \tilde{\chi}_1^+ \mu^- \\ & \searrow & \tilde{\chi}_1^0 W^+ \rightarrow e^+(\mu^+)\nu \\ & \searrow & \mu^\pm q \bar{q}' \end{array} \quad (2)$$

which presents a sequence of three decays which can be fully reconstructed. The strong kinematic constraint provided by the masses of the three sparticles in the cascade is sufficient to reduce the contribution of the different background sources well below the signal rate.

The signal events were generated with a version of the SUSYGEN Monte-Carlo [22] modified to allow the generation of pp processes. The hard-subprocess $q\bar{q}' \rightarrow \tilde{\chi}^\pm \mu^\mp$ is first generated according to the full lowest order matrix elements corresponding to the diagrams depicted in Figure 1. Cascade decays of the $\tilde{\chi}$'s are performed according to the relevant matrix elements. The parton showers approach [23] relying on the DGLAP [24] evolution equations is used to simulate QCD radiations in the initial and final states, and the non-perturbative part of the hadronization is modeled using string fragmentation [23]. The events were then processed through the program ATLFast [25], a parameterized simulation of the ATLAS detector response.

In this section, the analysis will be performed for the \mathcal{R}_p coupling $\lambda'_{211} = 0.09$ and for the following MSSM point:

$M_1 = 75$ GeV, $M_2 = 150$ GeV, $\mu = -200$ GeV, $\tan\beta = 1.5$, $A_t = A_b = A_\tau = 0$, $m_{\tilde{f}} = 300$ GeV.

For this set of MSSM parameters, the masses of the relevant gauginos are:

$$m_{\tilde{\chi}_1^0} = 79.9 \text{ GeV} \quad m_{\tilde{\chi}_1^\pm} = 162.3 \text{ GeV}$$

and the $\tilde{\chi}_1^\pm$ decay into an on shell W has a branching ratio of order 100%. The total cross-section for the resonant sneutrino production $pp \rightarrow \tilde{\nu}$ is 37 pb. If we include the branching fractions into the three leptons, the cross-section is 3.3 pb, corresponding to ~ 100000 events for the standard integrated luminosity of 30 fb^{-1} for the first three years of LHC data taking.

The signal is characterised by the presence of three isolated leptons and two jets. For the initial sample selection we require that:

- Exactly three isolated leptons are found in the event, with $p_T^1 > 20$ GeV, $p_T^{2,3} > 10$ GeV, where p_T is the momentum component in the plane perpendicular to the beam direction, and pseudorapidity $|\eta| < 2.5$.
- At least two of the three leptons must be muons.
- At least two jets with $p_T > 15$ GeV are found.
- The invariant mass of any $\mu^+\mu^-$ pair is outside ± 6.5 GeV of the Z mass.

The isolation prescription on the leptons is necessary to reduce the background from the semileptonic decays of heavy quarks, and consists in requiring an energy deposition of less than 10 GeV not associated with the lepton in a pseudorapidity-azimuth $(\eta - \phi)$ cone of opening $\Delta R = 0.2$ around the lepton direction.

The efficiency for these cuts, after the branching fractions have been taken into account, is $\sim 25\%$, where half of the loss comes from requiring three isolated leptons, and the other half is the loss of jets from $\tilde{\chi}_1^0$ decay either because they are not reconstructed, or because the two jets from the decay are reconstructed as a single jet. The Z mass cut gives a 10% loss in statistics. In order to avoid the combinatorial background from additional QCD events we further require that no third jet with $p_T > 15$ GeV is reconstructed in the event. The efficiency after this cut is $\sim 15\%$.

The reconstruction of the sparticle masses could be performed either starting from the $\tilde{\chi}_1^0$ reconstruction and going up the decay chain, or trying to exploit the three mass constraints at the same time. We choose the first approach which is not optimal, but allows a clearer insight into the kinematics of the events.

The first step in reconstruction of the $\tilde{\chi}_1^0 \rightarrow \mu$ jet jet is the choice of the correct muon to attempt the reconstruction. The three leptons come in the following flavour-sign configurations (+ charge conjugates):

1. $\mu^- e^+ \mu^+$
2. $\mu^- e^+ \mu^-$
3. $\mu^- \mu^+ \mu^+$
4. $\mu^- \mu^+ \mu^-$

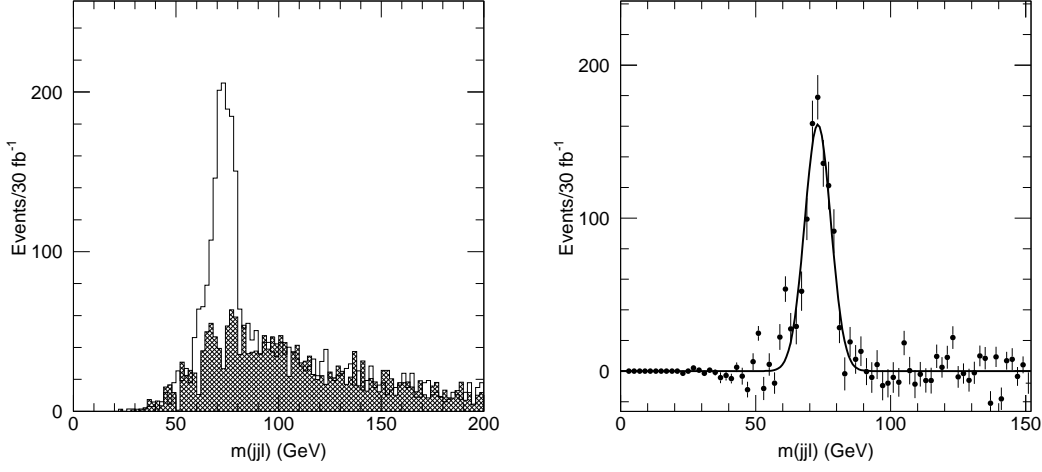


Figure 4: μ -jet-jet invariant mass for events in configuration 1. (see text) Left: exclusive two jet events with superimposed (hatched) the combinatorial background Right: $\tilde{\chi}_1^0$ peak after background subtraction.

where the first lepton comes from the $\tilde{\nu}_\mu$, the second one from the W , and the third one from the $\tilde{\chi}_1^0$ decay, corresponding to three final state signatures : 1) two opposite sign muons and an electron ¹, 2) two same-sign muons and an electron, 3-4) three muons. The configuration with three same-sign muons does not correspond to the required signature and is rejected in the analysis. For signature 1) the muon produced in the $\tilde{\chi}_1^0$ decay is defined as the one which has the same sign as the electron. For configuration 2) both muons must be tested to reconstruct the $\tilde{\chi}_1^0$. For configuration 3-4), the $\tilde{\chi}_1^0$ muon must be one of the two same-sign ones.

In order to minimise the combinatorial background we start the reconstruction from signature 1) where each lepton is unambiguously attributed to a step in the decay. The distribution of the μ -jet-jet invariant mass is shown in the left plot of Figure 4. A clear peak is visible corresponding to the $\tilde{\chi}_1^0$ mass superimposed to a combinatorial background of events where one of the two jets from the $\tilde{\chi}_1^0$ was lost and a jet from initial state radiation was picked up. The combinatorial background can be evaluated using three-jet events, where at least one jet is guaranteed to come from initial state radiation. The shape of the combinatorial background estimated with this method is shown as the shaded histogram superimposed to the signal peak. After background subtraction, an approximately gaussian peak with a width of ~ 4.5 GeV, and a statistics of about 1050 events

¹Here and in the following, “electron” stands for both e^+ and e^- .

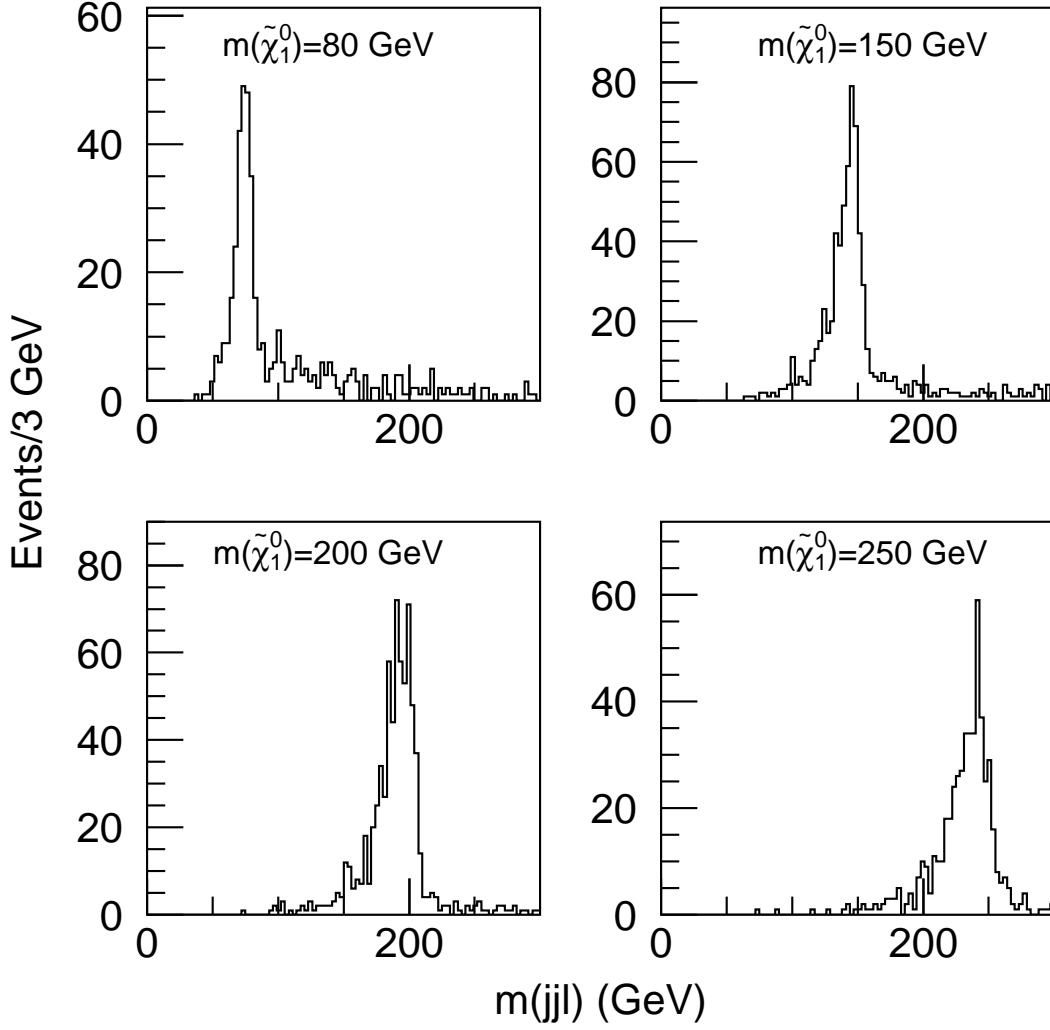


Figure 5: *Lepton-jet-jet invariant mass for exclusive two-jet events where the $\tilde{\chi}_1^0$ lepton is uniquely defined, for four different values of the $\tilde{\chi}_1^0$ mass: $m_{\tilde{\chi}_1^0}=80$, 150, 200 and 250 GeV. In all cases the sneutrino mass is set at 500 GeV, $-\mu = M_2 = 2M_1$, and $\tan\beta = 1.5$, yielding a $\tilde{\chi}_1^\pm$ mass twice the $\tilde{\chi}_1^0$ mass. All the sfermion masses are set to 500 GeV. The normalisation is arbitrary.*

is reconstructed, shown in the right of Figure 4. If we consider a window of ± 12 GeV around the peak, corresponding to $\sim 2.5\sigma$ of the gaussian, ~ 1500 events are observed in the sample, and the combinatorial contamination is approximately $\sim 30\%$. A tail towards low mass values is observed, corresponding to events where a fraction of the parton energy is lost in the jet reconstruction. From this distribution the $\tilde{\chi}_1^0$ mass can be measured with a statistical error of ~ 100 MeV. The measurement error will in this case be dominated by the systematic error on the jet energy scale which in ATLAS is estimated to be at the level of 1% [31].

The 30% combinatorial background is due to the 'soft' kinematics of the chosen example point, with a $\tilde{\chi}_1^0$ which is both light and produced with a small boost. In order to show the effect of the mass hierarchy of the involved sparticles, the shape of the $\tilde{\chi}_1^0$ mass peak is shown in Figure 5 for a sneutrino mass of 500 GeV and different choices for the $\tilde{\chi}_1^0$ mass. In all cases the $\tilde{\chi}_1^\pm$ mass is twice the $\tilde{\chi}_1^0$ mass, corresponding to the gauge unification condition and to $|\mu|$ values of the same order as M_2 . The combinatorial background is in general smaller than for a 300 GeV sneutrino, due to the higher boost imparted to the $\tilde{\chi}_1^0$, and it decreases with increasing $\tilde{\chi}_1^0$ masses, due to the higher efficiency for reconstructing both jets from the $\tilde{\chi}_1^0$ decay. For this analysis no attempt has been done for the recalibration of the jet energy. This results in the skewing of the distributions towards low masses, and in the peak value being slightly displaced with respect to the nominal mass value.

Once the position of the $\tilde{\chi}_1^0$ mass peak is known, the reconstructed $\tilde{\chi}_1^0$ statistics can be increased by also considering signatures 2) and 3-4). For events coming from signatures 2 to 4, the $\tilde{\chi}_1^0$ candidate is defined as the muon-jet-jet combination which gives a mass nearest to the mass peak determined from signature 1) events. In all cases the reconstructed mass is required to be within ± 12 GeV of the peak position to define a $\tilde{\chi}_1^0$ candidate. In 83% of the events containing at least a combination satisfying this requirement, only one $\tilde{\chi}_1^0$ candidate is found, and this sample can be used to improve the statistical precision on the $\tilde{\chi}_1^0$ mass measurement.

Using the above definition of the $\tilde{\chi}_1^0$, we can go further in the mass reconstruction of the involved sparticles. Only configurations 1) and 2) are used, i.e. the events containing two muons and an electron in order to avoid ambiguities in the choice of the lepton from the W decay. The preliminary step for the reconstruction of the $\tilde{\chi}_1^\pm$ is the reconstruction of the W boson from its leptonic decay. The longitudinal momentum of the neutrino from the W decay is calculated from the missing transverse momentum of the event (considered as p_T^ν) and the requirement that the electron-neutrino invariant mass gives the W mass. The resulting neutrino longitudinal momentum, has a twofold ambiguity. We therefore build the invariant $W - \tilde{\chi}_1^0$ mass candidate using both solutions for the W boson momentum. The resulting spectrum is shown in Figure 6, as the full line

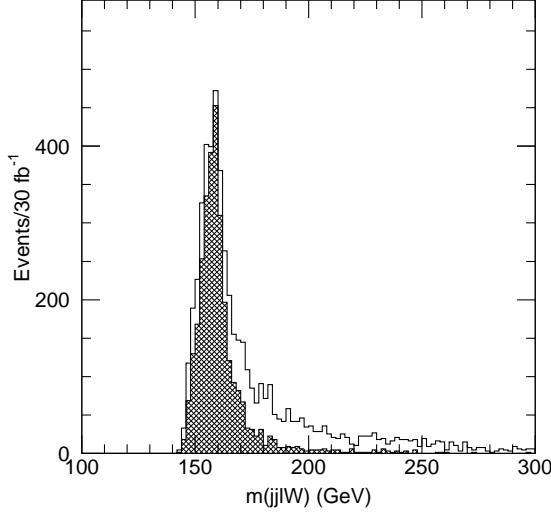


Figure 6: *Invariant mass of the $\tilde{\chi}_1^0$ with the W candidate. The full line histogram includes both solutions for the neutrino longitudinal momentum, the grey one only includes the solution which gives the mass nearest to the measured peak.*

histogram. A clear peak is seen, superimposed on a combinatorial background. If only the solution yielding the $\tilde{\chi}_1^\pm$ mass nearest to the measured mass peak is retained, the mass spectrum corresponding to the shaded histogram is obtained. The peak in the unbiased histogram can be fitted with a gaussian shape, with a width of ~ 6 GeV.

The combination with the mass nearest to the measured peak is taken as $\tilde{\chi}_1^\pm$ candidate, provided that the reconstructed mass is within 15 GeV of the peak. For 80% of the $e\mu\mu$ events where a $\tilde{\chi}_1^0$ candidate is found, a $W - \tilde{\chi}_1^0$ combination satisfying this requirement is reconstructed.

Finally the $\tilde{\chi}_1^\pm$ candidates are combined with the leftover muon, yielding the mass spectrum shown in Figure 7. The $\tilde{\nu}$ mass peak at this point presents very limited tails, and has a width of ~ 10 GeV. We define fully reconstructed events as those for which this mass lies within 25 GeV of the measured $\tilde{\nu}$ peak. From the estimate of the combinatorial under the $\tilde{\chi}_1^0$ peak, we expect approximately $2 \times 1050 = 2100$ events where all the jets and leptons are correctly assigned over a total of 2450 events observed in the peak. The difference between the two numbers are events for which one of the two jets used for the $\tilde{\chi}_1^0$ reconstruction comes from initial state radiation. These jets are typically soft, and therefore the reconstructed $\tilde{\chi}_1^0$ candidate very often has a momentum which both in magnitude and direction is close to the momentum of the original $\tilde{\chi}_1^0$. Therefore for such

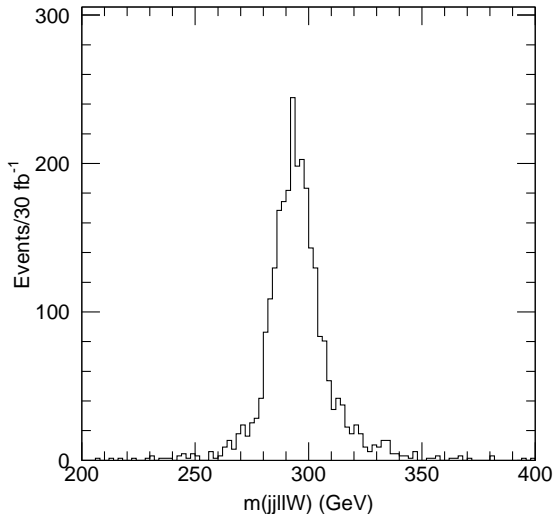


Figure 7: *Invariant mass of the third lepton in the event with the $\tilde{\chi}_1^\pm$ candidate.*

events the reconstructed $\tilde{\chi}_1^0$ behaves in the further steps in the reconstruction as the real one, only inducing some widening in the $\tilde{\chi}_1^\pm$ and $\tilde{\nu}$ peaks.

The statistics available at the different steps in the analysis for an integrated luminosity of 30 fb^{-1} is given in the first column of Table 1. For the assumed value of the coupling, $\lambda'_{211} = 0.09$, the uncertainty on the measurement of all the three masses involved will be dominated by the 1% uncertainty on the jet energy scale.

The efficiency for the reconstruction of the full decay chain with the analysis described above is $\sim 2.5\%$. A more sophisticated analysis using also the three-muons events should approximately double this efficiency.

From the observed number of events and the $\tilde{\nu}$ mass a measurement of the quantity $\lambda_{211}^2 \times BR$, where BR is the product of the branching ratios of the decays shown in equation 2, is possible. The measurement of additional SUSY processes will be needed to disentangle the two terms of this product.

3.2 Standard Model Background

The requirement of three isolated leptons in the events strongly reduces the possible background sources. The following processes were considered as a background:

- $t\bar{t}$ production, followed by $t \rightarrow Wb$, where the two W and one of the b

Process	Signal	$t\bar{t}$	WZ	Wbb	Wt	Zb
σ (pb)	3.3	590	26	300	60	7000
$N_{ev}(30 \text{ fb}^{-1})$	1×10^5	1.7×10^7	8×10^5	9×10^6	1.8×10^6	2.1×10^8
Loose cuts	23600	2900	53	2.4	3.5	56
Jet veto	14200	1450	38	-	-	30
$\tilde{\chi}_1^0$	6750	158	4	-	-	-
$\tilde{\chi}_1^\pm$	2700	8	0.4	-	-	-
$\tilde{\nu}_\mu$	2450	0	0.25	-	-	-

Table 1: *Cross-sections and expected numbers of events after cuts for the signal and the different Standard Model background contributions considered in the analysis. The “Loose cuts” are described at the beginning of section 3.1, and the “Jet veto” consists in adding the requirement that no third jet with $p_T > 15$ GeV is reconstructed in the event. The line labelled “ $\tilde{\chi}_1^0$ ” gives the number of events from signatures 1 to 4 ($e\mu\mu$ and $\mu\mu\mu$) for which a $\tilde{\chi}_1^0$ candidate is found. The line labelled “ $\tilde{\chi}_1^\pm$ ” shows the number of events from signatures 1 and 2 ($e\mu\mu$) where a $\tilde{\chi}_1^\pm$ candidate is found in addition, and the last line indicates the number of fully reconstructed events. In the case of the signal, we give the cross-section for the resonant sneutrino production multiplied by the branching ratios into three leptons.*

quarks decay leptonically.

- WZ production, where both bosons decay leptonically.
- Wt production
- Wbb production
- Zb production

These backgrounds were generated with the PYTHIA MonteCarlo [26], except Wt and Wbb for which the ONETOP parton level generator [27] was used, interfaced to PYTHIA for hadronisation and fragmentation. The cross-sections for the various processes, and the number of total expected events for an integrated luminosity of 30 fb^{-1} are given in Table 1, according to the cross-section numbers used in the ATLAS physics performance TDR [31]. In particular, even when the cross-section is known at NLO, as in the case of the top, the Born cross-section is taken for internal consistency of the study.

For each of the background processes a sample of events between one seventh and a few times the expected statistics was generated and passed through the simplified simulation of the ATLAS detector.

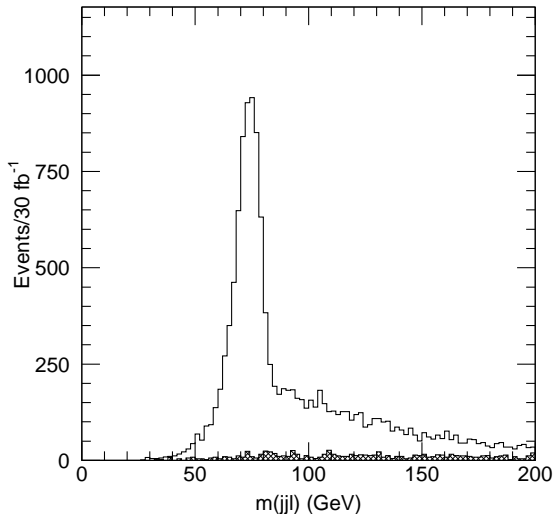


Figure 8: *Invariant mass of the $\tilde{\chi}_1^0$ candidates entering the kinematic analysis superimposed to the Standard Model background (hatched).*

After the loose selection cuts described in Section 3.1, the background is dominated by top production, as can be seen from the numbers shown in Table 1. The distribution of the μ -jet-jet invariant mass for background events, obtained as in Section 3.1 and corresponding to the $\tilde{\chi}_1^0$ candidates selection, is shown as the hatched histogram in Figure 8. In this figure we have superimposed the same distribution for the signal. Already at this level, the signal stands out very clearly from the background, and in the following steps of the reconstruction the background becomes almost negligible. The numbers of background and signal events expected at the various steps of the reconstruction can be compared in Table 1. The full analysis was performed only for the $\bar{t}t$ and WZ background because for the other channels the background is essentially negligible compared to top production, and in most cases the MonteCarlo statistics after the initial selection was too low to allow a detailed study. For the SUSY model considered and the chosen value of the λ' coupling constant, even the loose selection applied allows to efficiently separate the signal from the background.

3.3 Sensitivity on λ'

From these results, it is possible to evaluate the minimum value of the λ'_{211} coupling for which it will be possible to discover the signal. The starting point in

the analysis is the observation of a peak in the muon-jet-jet invariant mass over an essentially flat background. All of the further analysis steps of the cascade reconstruction rely on the possibility of selecting the events with a mass around the $\tilde{\chi}_1^0$ peak.

For the observation of the peak, the best signal/background ratio is obtained using the three-muons sample (configurations 3 and 4 above). In the Standard Model, which incorporates lepton universality, about one eighth of the three-leptons events present a three-muons configuration, whereas about half of the signal events come in this configuration, thereby granting an improvement of a factor 4 in signal over background, with respect to the full sample. The three muons come either in the ‘- + +’ or in the ‘- + -’ sign configuration, because the two muons from the decay chain $\tilde{\nu}(\tilde{\bar{\nu}}) \rightarrow \tilde{\chi}_1^\pm \mu^\mp \rightarrow \tilde{\chi}_1^0 \mu^\pm \mu^\mp$ must have opposite sign, whereas the $\tilde{\chi}_1^0$ can decay to muons of either sign. Therefore the muon for the $\tilde{\chi}_1^0$ reconstruction must be chosen between the two same-sign ones. The

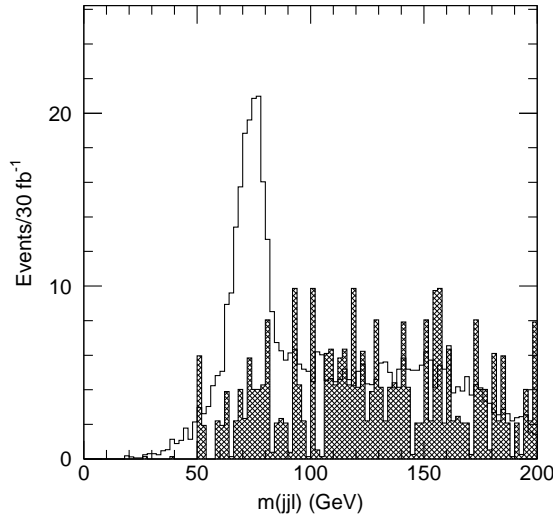


Figure 9: *Invariant mass of the $\tilde{\chi}_1^0$ candidates from three-muon events scaled down by a factor 25, corresponding to a λ' value of 0.018, superimposed to the Standard Model background (hatched).*

distribution for the μ -jet-jet invariant mass, for events containing two jets and three muons is shown in Figure 9, scaled down by a factor 25, corresponding to a λ' value of 0.018, superimposed to the expected top background. In the distribution each event enters twice, for each of the two same-sign muons which can be used to reconstruct the $\tilde{\chi}_1^0$. We expect, however, that the combination with the “wrong” muon gives in most cases a reconstructed mass outside of the $\tilde{\chi}_1^0$ peak.

A statistical prescription is needed to define the fact that a peak structure is seen in the signal+background distribution. Given the exploratory nature of the work, we adopt the naive approach of calculating the λ' value for which $S/\sqrt{B} = 5$, where S and B are respectively the number of signal and background candidates counted in an interval of ± 15 GeV around the measured $\tilde{\chi}_1^0$ peak. The window for the definition of a $\tilde{\chi}_1^0$ candidate is enlarged with respect to the analysis described in Section 3.1, in order to recover the non-gaussian tail of the signal peak, thus increasing the analysis efficiency. In this interval, for the chosen point, for an integrated luminosity of 30 fb^{-1} , $S = 580000 \times (\lambda')^2$ and $B = 46$ events. In the hypothesis that the $\bar{t}t$ background can be precisely measured from data, the lower limit on λ'_{211} is:

$$\lambda'_{211} > 0.0075$$

The pair production of SUSY particles through standard R_p -conserving processes is another possible source of background, due to the possibility to obtain final states with high lepton multiplicity, and the high production cross-sections. This background can only be evaluated inside models providing predictions for the whole SUSY spectrum. As a preliminary study, a sample of events were generated with the HERWIG 6.0 MonteCarlo [29] by setting the slepton masses at 300 GeV, the masses of squarks and gluinos at 1000 GeV and the chargino-neutralino spectrum as for the example model. The total R_p -conserving cross-section is in this case $\sim 6 \text{ pb}$. A total of 60 SUSY background events which satisfy the requirements used above to define S and B are observed. All the events surviving the cuts are from direct chargino and neutralino production, with a small contribution from Drell-Yan slepton production. Since the contributions from squark and gluino decays are strongly suppressed by the jet veto requirements, this result can be considered as a correct order of magnitude estimate, independently from the assumed values for the squark and gluino masses. Moreover, the reconstructions of the chargino and sneutrino masses can also be used in order to reduce the SUSY background. A more thorough discussion of the SUSY background will be given below in the framework of the mSUGRA model.

4 Analysis reach in various models

For the example case studied in Section 3.1 it was shown that the sneutrino production signal can be easily separated from the background, and allows to perform precision measurements of the masses of the sparticles involved in the decay chain.

The analysis can be generalised to investigate the range of SUSY parameters in which this kind of analysis is possible, and to define the minimum value of the λ'

constant which gives a detectable signal in a given SUSY scenario. The different model parameters enter the definition of the detectability at different levels:

- The sneutrino production cross-section is a function only of the sneutrino mass and of the square of the R-parity violating coupling constant.
- The branching fraction of the sneutrino decay into three leptons is a function of all the SUSY parameters.
- The analysis efficiency is a function of the masses of the three supersymmetric particles involved in the decay.

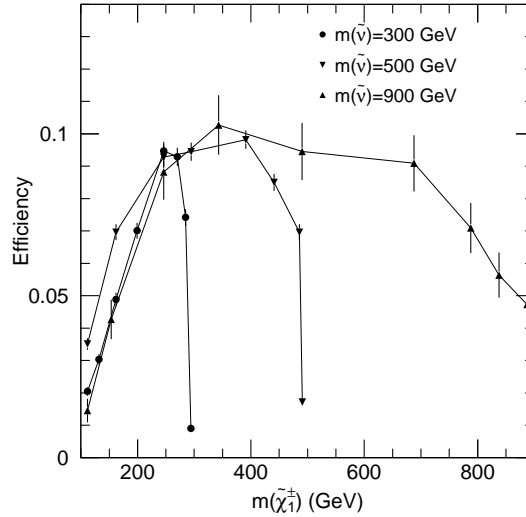


Figure 10: *Efficiency for reconstructing a μ -jet-jet invariant mass within 15 GeV of the $\tilde{\chi}_1^0$ mass in three-muons events, as a function of the $\tilde{\chi}_1^\pm$ mass. The shown points were generated with the following parameters: $-\mu = M_2 = 2M_1$, $\tan\beta = 1.5$. All the sfermion masses are set equal to the sneutrino mass. Points for $m_{\tilde{\nu}} = 300, 500$ and 900 GeV are shown.*

The dependences of the cross-section and branching ratios on the SUSY parameters were discussed in Section 2 for the MSSM, and are summarised in Figures 2 and 3. We only need at this point to parameterize the analysis efficiency as a function of the sparticle masses. The number of signal events for each considered model will then be obtained by multiplying the expected number of three-lepton events by the parameterized efficiency.

4.1 Efficiency of the three-muon analysis

According to the discussion presented in Section 3.3, we need to calculate the efficiency for the signal process to satisfy the following requirements:

- to pass the initial selection cuts described in Section 3.1 (Loose cuts), including the veto on the third jet (Jet veto);
- to contain three reconstructed muons, with one of the μ -jet-jet invariant masses within 15 GeV of the $\tilde{\chi}_1^0$ mass.

Three sneutrino masses, $m_{\tilde{\nu}} = 300, 500$ and 900 GeV were considered, and for each of these the evolution of the efficiency with the $\tilde{\chi}_1^\pm$ mass was studied. The mass of the $\tilde{\chi}_1^0$ was assumed to be half of the mass of the $\tilde{\chi}_1^\pm$, relation which is in general valid in SUGRA inspired models and correspond to a choice of values for $|\mu|$ of the same order as M_2 .

The analysis efficiency is shown in Figure 10 as a function of the $\tilde{\nu}_\mu$ mass and of the $\tilde{\chi}_1^\pm$ mass. The efficiency values are calculated with respect to the number of events which at generation level did contain the three leptons, therefore they only depend on the event kinematics and not on the branching ratios. The loss of efficiency at the lower end of the $\tilde{\chi}_1^\pm$ mass spectrum is due to the inefficiency for detecting two jets from the $\tilde{\chi}_1^0$ decay, either because the two jets are reconstructed as a single jet, or because one of the two jets is below the detection threshold of 15 GeV. The efficiency then becomes approximately independent of the masses of the sneutrino and of the $\tilde{\chi}_1^\pm$, up to the point where the $\tilde{\nu}$ and $\tilde{\chi}_1^\pm$ masses become close enough to affect the efficiency for the detection of the muon from the $\tilde{\nu} \rightarrow \tilde{\chi}_1^\pm \mu$ decay; for $m_{\tilde{\nu}} - m_{\tilde{\chi}_1^\pm} < 10$ GeV the analysis efficiency rapidly drops to zero. The moderate decrease in efficiency at high $\tilde{\chi}_1^\pm$ masses for $m_{\tilde{\nu}} = 900$ GeV can be ascribed to the fact that one of two energetic jets from the $\tilde{\chi}_1^0$ decay radiates a hard gluon, three jets are reconstructed, and the event is rejected by the jet veto.

At this point all the ingredients are available to study the reach in the parameter space for the analysis presented in Section 3 within different SUSY models.

4.2 Analysis reach in the MSSM

The region in the $m_{\tilde{\nu}}-m_{\tilde{\chi}_1^\pm}$ plane for which the signal significance is greater than 5σ , as defined in Section 3.3, and at least 10 signal events are observed for an integrated luminosity of 30 fb^{-1} is shown in Figure 11 for different choices of the

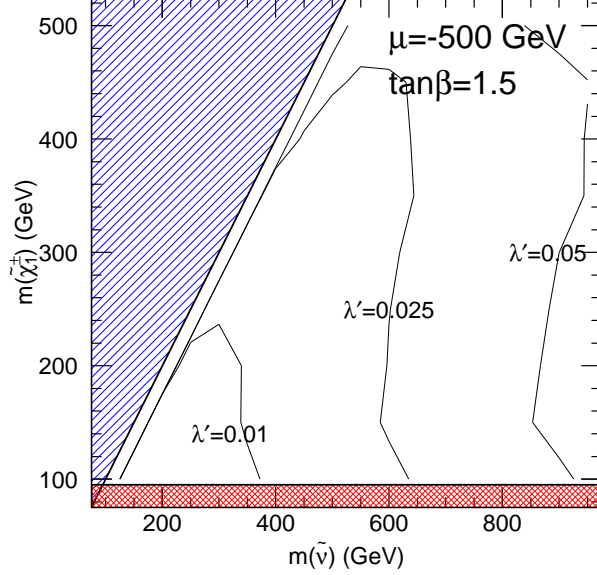


Figure 11: 5σ reach in the $m_{\tilde{\nu}}-m_{\tilde{\chi}_1^\pm}$ plane for three different choices of the λ'_{211} coupling for an integrated luminosity of 30 fb^{-1} at the LHC. The chosen model parameters were: $\mu = -500 \text{ GeV}$, $\tan\beta=1.5$, $m_{\tilde{q}} = m_{\tilde{l}} = 300 \text{ GeV}$, $A_t = A_b = A_\tau = 0$, $M_2 = 2M_1$. The significance is defined only considering the Standard Model background, and a signal of at least ten events is required. The hatched region at the upper left corresponds to $m_{\tilde{\nu}} < m_{\tilde{\chi}_1^\pm}$. The cross-hatched region at low $m_{\tilde{\chi}_1^\pm}$ is excluded by the preliminary LEP results at $\sqrt{s} = 196 \text{ GeV}$ [30].

λ'_{211} constant. The behaviours of the sensitivity curves in the $m_{\tilde{\nu}}-m_{\tilde{\chi}_1^\pm}$ plane are well explained by the variations of the single chargino production cross-section shown in Figure 3 in the same plane of parameters. The SUSY background is not considered in the plot, as it depends on all the model parameters. It was however verified in a few example cases that for our analysis cuts this background is dominated by direct chargino and neutralino production, and it becomes negligible in the limit of high $\tilde{\chi}_1^0$ and $\tilde{\chi}_1^\pm$ masses. The main effect of taking into account this background will be to reduce the significance of the signal for $\tilde{\chi}_1^\pm$ masses lower than 200 GeV.

From the curves in Figure 11 we can conclude that within the MSSM, the production of a 900 GeV sneutrino for $\lambda'_{211} > 0.05$, and of a 350 GeV sneutrino for $\lambda'_{211} > 0.01$ can be observed within the first three years of LHC running,

λ'_{211}	λ'_{212}	λ'_{213}	λ'_{221}	λ'_{222}	λ'_{223}	λ'_{231}	λ'_{232}	λ'_{233}
0.01	0.02	0.02	0.02	0.03	0.05	0.03	0.06	0.09

Table 2: *Sensitivities on the λ'_{2jk} coupling constants deduced from the sensitivity on λ'_{211} for $\tan\beta=1.5$, $M_1 = 100$ GeV, $M_2 = 200$ GeV, $\mu = -500$ GeV, $m_{\tilde{q}} = m_{\tilde{l}} = 300$ GeV and $m_{\tilde{\nu}} = 400$ GeV.*

provided that the sneutrino is heavier than the lightest chargino.

The sensitivity on an \mathcal{R}_p coupling of type λ'_{2jk} can be derived from the sensitivity obtained for λ'_{211} , as explained in Section 2.2. For example, we have seen that the sensitivity on λ'_{221} was ~ 1.5 times weaker than the sensitivity on λ'_{211} , for $\tan\beta=1.5$, $M_2 = 200$ GeV, $\mu = -500$ GeV and $m_{\tilde{\nu}} = 400$ GeV. This set of parameters leads to a sensitivity on λ'_{211} of about 0.015 as can be seen in Figure 11, and hence to a sensitivity on λ'_{221} of ~ 0.022 . In Table 2, we present the sensitivity on any λ'_{2jk} coupling estimated using the same method and for the same MSSM parameters. Those sensitivities represent an important improvement with respect to the low-energy limits of [1].

In the case of a single dominant λ'_{2j3} coupling the neutralino decays as $\tilde{\chi}_1^0 \rightarrow \mu u_j b$ and the semileptonic decay of the b-quark could affect the analysis efficiency. Hence in this case, the precise sensitivity cannot be simply calculated by scaling the value obtained for λ'_{211} . The order of magnitude of the sensitivity which can be inferred from our analysis should however be correct.

4.3 Analysis reach in mSUGRA

Our framework throughout this Section will be the so-called minimal supergravity model. In this model the parameters obey a set of boundary conditions at the Grand Unification Theory (GUT) scale M_x . These conditions appear to be natural in supergravity scenario since the supersymmetry breaking occurs in an hidden sector which communicates with the visible sector only through gravitational interactions. First, mSUGRA contains the gauge coupling unification at M_x , such an unification being suggested by the experimental results obtained at LEP I. One can view the gauge coupling unification assumption as a fixing of the GUT scale M_x . Second, the gaugino (bino, wino and gluino) masses at M_x are given by the universal mass $m_{1/2}$. the parameters $m_{1/2}$ and M_i [$i = 1, 2, 3$] are thus related by the solutions of the renormalization group equations (RGE). Besides, since the gaugino masses and the gauge couplings are governed by the same RGE, one has the well-known relation: $M_1 = \frac{5}{3} \tan^2 \theta_W M_2$. Similarly, at M_x , the universal scalars mass is m_0 and the trilinear couplings are all equal to A_0 . Finally, in mSUGRA the absolute value of the higgsino mixing parameter

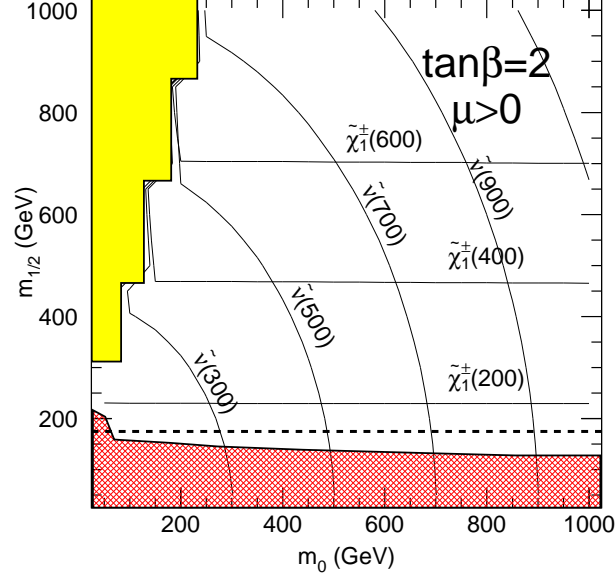
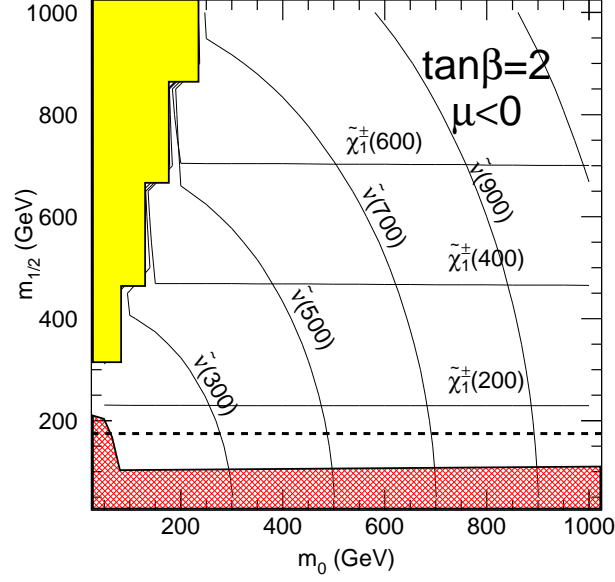


Figure 12: Curves of equal mass for $\tilde{\nu}$ and $\tilde{\chi}_1^\pm$ in the m_0 – $m_{1/2}$ plane for $\tan\beta = 2$. The grey region at the upper left indicates the domain where the $\tilde{\chi}_1^0$ is not the LSP. The cross-hatched region for low $m_{1/2}$ gives the kinematic limit for the discovery of $\tilde{\chi}_1^\pm$ or \tilde{l} by LEP running at $\sqrt{s} = 200$ GeV. The dotted line shows the region below which the $\tilde{\chi}_1^\pm$ decays to a virtual W .

$|\mu|$ as well as the bilinear coupling B are determined by the radiative electroweak symmetry breaking conditions. Therefore, mSUGRA contains only the five following parameters: $\text{sign}(\mu)$, $\tan\beta$, A_0 , m_0 and $m_{1/2}$.

Due to the small dependence of the single chargino production rate on the μ parameter for $M_2 \leq |\mu|$ (see Section 2), the study of the mSUGRA model in which $|\mu|$ is fixed by the electroweak symmetry breaking condition provides information on a broader class of models. The single chargino production rate depends mainly on the values of m_0 and $m_{1/2}$ (see Section 2). We will set $A_0 = 0$, and study the detectability of the signal in the $m_0 - m_{1/2}$ plane. We show in Figure 12 the curves of equal mass for $\tilde{\nu}$ and $\tilde{\chi}_1^\pm$ for $\tan\beta = 2$ calculated with the ISASUSY [28] package which uses one-loop RGE to get the SUSY spectrum from the mSUGRA parameters.

The signal reach can be easily evaluated from the sparticle mass spectrum and branching fractions by using the parameterization of the analysis efficiency shown in Figure 10.

4.3.1 Supersymmetric background

In the case of a well constrained model as mSUGRA, the SUSY background can in principle be evaluated in each considered point in the parameter space. For this evaluation the full SUSY sample must be generated for each point, requiring the generation of a large number of events.

The sparticle masses for the model studied in detail in Section 3 uniquely define a model in the mSUGRA framework. Therefore, as a first approach to the problem, a full analysis was performed for this model, corresponding to the parameter values:

$$m_0 = 275 \text{ GeV}, \quad m_{1/2} = 185 \text{ GeV}, \quad \tan\beta = 1.5, \quad \mu < 0, \quad A_0 = 0.$$

For this mSUGRA point, the mass scale for squarks/gluinos is in the proximity of 500 GeV, and the total cross-section for all the SUSY particles pair productions is approximately 130 pb, yielding a signal of $\sim 4 \cdot 10^6$ events for the first three years of data-taking at the LHC. A total of 400k events were generated and analysed. The number of surviving events after cuts in the three-muons sample was 47 ± 21 for an integrated luminosity of 30 fb^{-1} . All the background events come from direct chargino and neutralino production, as it was the case for the MSSM point studied in Section 3.3. As a cross-check, we generated for the same mSUGRA point only the processes of the type $pp \rightarrow \tilde{\chi} + X$, where $\tilde{\chi}$ denotes either $\tilde{\chi}^0$ or $\tilde{\chi}^\pm$, and X any other SUSY particle. The cross-section is in this case $\sim 6 \text{ pb}$,

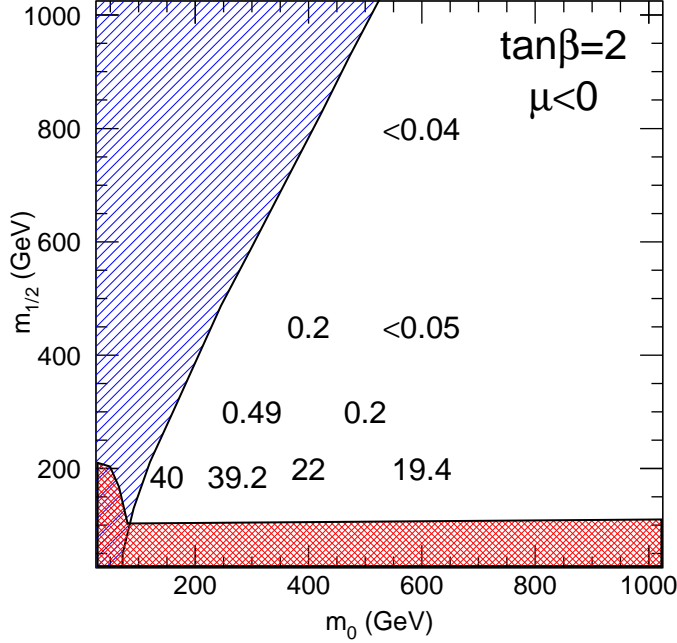


Figure 13: Number of SUSY background events for an integrated luminosity of 30 fb^{-1} in the $m_0 - m_{1/2}$ plane with $\tan \beta = 2$ for a few selected test models. The hatched region at the upper left corresponds to $m_{\tilde{\nu}} < m_{\tilde{\chi}_1^\pm}$. The cross-hatched region for low $m_{1/2}$ gives the kinematic limit for the discovery of $\tilde{\chi}_1^\pm$ or \tilde{l} by LEP running at $\sqrt{s} = 200 \text{ GeV}$.

and the number of background events is 39 ± 7 events, in good agreement with the number evaluated generating all the SUSY processes.

Based on this result, we have performed a scan in the $m_0 - m_{1/2}$ plane the fixed values $\tan \beta = 2$, $\mu < 0$. On a grid of points we generated event samples for the $pp \rightarrow \tilde{\chi} + X$ processes with the HERWIG 6.0 MonteCarlo [29]. The number of SUSY events with a μ -jet-jet combination with an invariant mass within 15 GeV of the $\tilde{\chi}_1^0$ mass is shown in Figure 13 in the $m_0 - m_{1/2}$ plane for an integrated luminosity of 30 fb^{-1} . The background is significant for a $\tilde{\chi}_1^\pm$ mass of 175 GeV ($m_{1/2} = 200 \text{ GeV}$), and becomes essentially negligible for $\tilde{\chi}_1^\pm$ mass of 260 GeV ($m_{1/2} = 300 \text{ GeV}$). This behaviour is due to the combination of two effects: the $\tilde{\chi}^\pm \tilde{\chi}^\pm$ production cross-section decreases with increasing $\tilde{\chi}^\pm$ mass, and the probability of losing two of the four jets from the decay of the two $\tilde{\chi}_1^0$ in the event becomes very small for a $\tilde{\chi}_1^\pm$ mass of $\sim 220 \text{ GeV}$. Indeed, the

suppression of the SUSY background is mainly due to the Jet veto cut.

Given the high SUSY cross-section, and the high lepton multiplicity from $\tilde{\chi}_1^0$ decays, a prominent signal should manifest itself through R-conserving sparticle pair production in this scenario. Single resonant sneutrino production will then be used as a way of extracting information on the value of the R_p -violating coupling constant, and of precisely measuring the masses of $\tilde{\nu}_\mu$, $\tilde{\chi}_1^\pm$, $\tilde{\chi}_1^0$. Moreover, thanks to the very high number of produced $\tilde{\chi}_1^0$ expected from \tilde{q}/\tilde{g} pair production, the $\tilde{\chi}_1^0$ mass will be directly reconstructed from \tilde{q} and \tilde{g} decays, as shown in [31]. So, for the present analysis it can be assumed that the $\tilde{\chi}_1^0$ mass is approximately known, and an attempt to reconstruct the $\tilde{\chi}_1^\pm$ peak can be performed even if the $\tilde{\chi}_1^0$ reconstruction does not yield a significant peak over the SUSY+SM background. In order to perform the full reconstruction, one just needs to observe a statistically significant excess of events over what is expected from the Standard Model background in the mass region corresponding to the known $\tilde{\chi}_1^0$ mass. The full kinematic reconstruction described in Section 3.1 above will then easily allow to separate the process of interest from the SUSY background.

4.3.2 Results

Based on the discussion in the previous section we calculate the signal significance as S/\sqrt{B} , where for the signal S we only consider the resonant sneutrino production, and for the background B we only consider the SM background. We show in Figure 14 for $\tan\beta = 2$ and for the two signs of μ the regions in the $m_0 - m_{1/2}$ plane for which the signal significance exceeds 5σ and the number of signal events is larger than 10, for an integrated luminosity of 30 fb^{-1} . The reach is shown for three different choices of the λ'_{211} parameter: $\lambda'_{211} = 0.01, 0.025, 0.05$. Even for the lowest considered coupling the signal can be detected in a significant fraction of the parameter space. The dotted line shows the region below which the $\tilde{\chi}_1^\pm$ decays to the $\tilde{\chi}_1^0$ and a virtual W , thus making the kinematic reconstruction of the decay chain described in Section 3.1 impossible. The reconstruction of the $\tilde{\chi}_1^0$ is however still possible, but the reconstruction efficiency drops rapidly due to the difficulty to separate the two soft jets from the $\tilde{\chi}_1^0$ decay. A detailed study involving careful consideration of jet identification algorithms is needed to assert the LHC reach in that region.

As observed in [32], the efficiencies quoted for this analysis rely on a branching ratio of $\sim 100\%$ for the decay $\tilde{\chi}_1^\pm \rightarrow W\tilde{\chi}_1^0$. This is in general true in SUGRA models as long as the $\tilde{\tau}_1$ is heavier than the $\tilde{\chi}_1^\pm$, corresponding to moderate values for $\tan\beta$. For high $\tan\beta$, the decay $\tilde{\chi}_1^\pm \rightarrow \tilde{\tau}_1\nu_\tau$ can become kinematically possible, and its branching ratio can dominate the standard $\tilde{\chi}_1^\pm \rightarrow W\tilde{\chi}_1^0$. The stau in turns typically decays as $\tilde{\tau}_1 \rightarrow \tau\tilde{\chi}_1^0$. The three-leptons signature is in

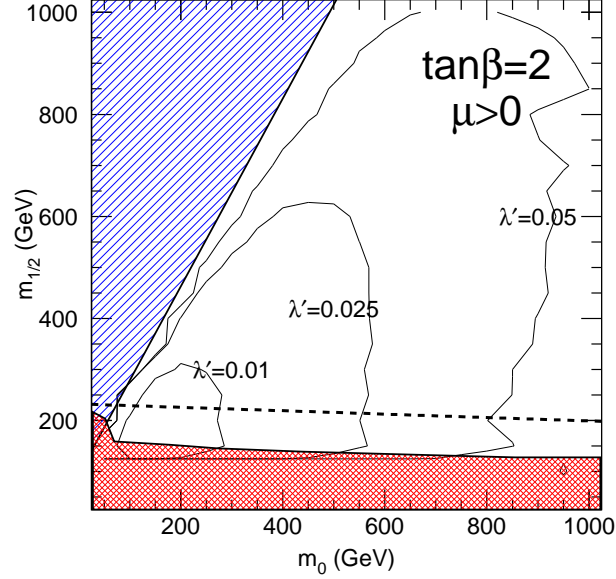
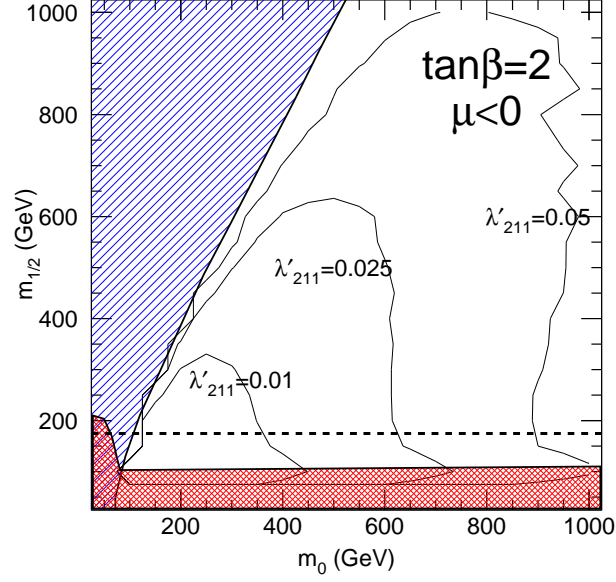


Figure 14: 5σ reach in the $m_0 - m_{1/2}$ plane for $\tan\beta=2$ and three different choices of the λ'_{211} coupling for an integrated luminosity of 30 fb^{-1} at the LHC. The significance is defined only considering the Standard Model background, and a signal of at least ten events is required. The dotted line shows the region below which the $\tilde{\chi}_1^\pm$ decays to a virtual W .

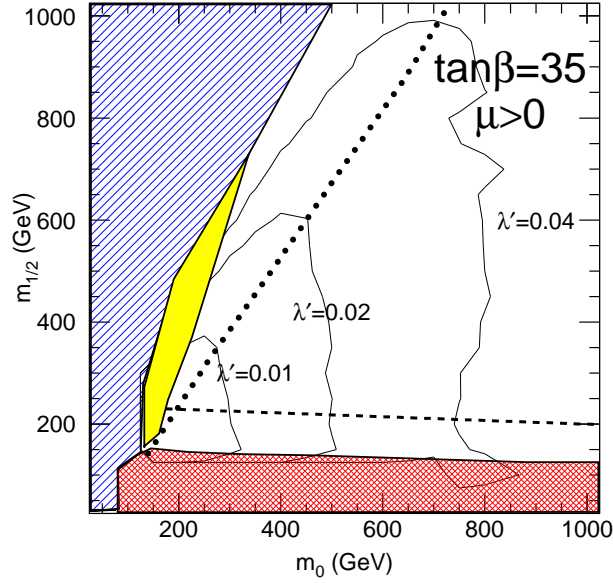
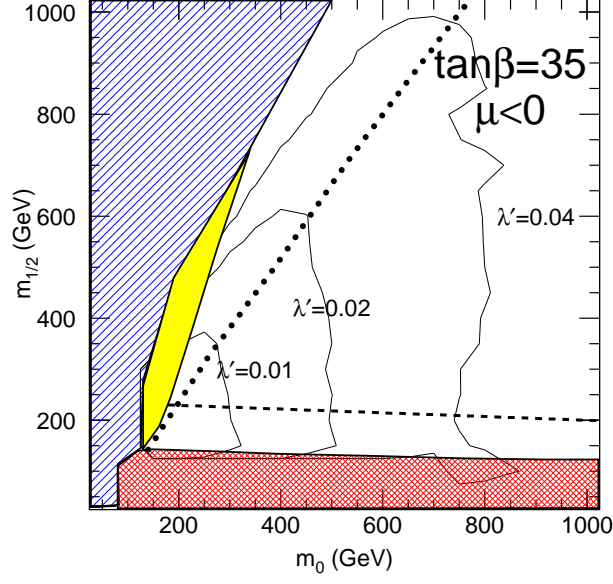


Figure 15: 5σ reach in the $m_0 - m_{1/2}$ plane for $\tan\beta=35$ and three different choices of the λ'_{211} coupling for an integrated luminosity of 30 fb^{-1} at the LHC. The significance is defined only considering the Standard Model background, and a signal of at least ten events is required. The dashed line shows the region below which the $\tilde{\chi}_1^\pm$ decays to a virtual W . The region to the left of the dotted lines has a branching ratio for $\tilde{\chi}_1^\pm \rightarrow \tilde{\tau}_1 \nu_\tau$ larger than 50%, and the grey area indicates the region for which a low signal efficiency is expected.

this case even enhanced, due to the higher branching fraction into electrons and muons for the τ compared to the W , at the price of a softer lepton spectrum. The $\tilde{\chi}_1^0$ reconstruction is still possible but the presence of three neutrinos (two additional neutrinos come from the leptonic τ decay) renders the reconstruction of the particles earlier in the decay chain difficult. The analysis efficiency is essentially unaffected with respect to the low $\tan\beta$ case as long as the mass difference between the $\tilde{\tau}_1$ and the $\tilde{\chi}_1^0$ is larger than ~ 50 GeV. For $\tilde{\tau}_1$ and $\tilde{\chi}_1^0$ masses too much degenerate, the transverse momentum of the charged lepton coming from the τ decay would often fall below the analysis requirements, leading thus to a reduction of the signal efficiency. The reach in the $m_0 - m_{1/2}$ plane is shown in Figure 15 for $\tan\beta = 35$ and three different choices of the λ'_{211} coupling. The branching fraction for the decay $\tilde{\chi}_1^\pm \rightarrow \tilde{\tau}_1 \nu_\tau$ is higher than 50% to the left of the dotted line, and the region for which a reduced signal efficiency is expected is displayed as a grey area. The reach for $\tilde{\chi}_1^0$ detection is similar to the low $\tan\beta$ case, but the region in which the full reconstruction of the sneutrino decay chain is possible is severely restricted.

5 Conclusions

We have analysed the resonant sneutrino production at LHC in supersymmetric models with R-parity violation. We have focused on the three-leptons signature which has a small Standard Model background, and allows a model-independent mass reconstruction of the full sneutrino decay chain.

A detailed study for an example MSSM point has shown that the mass reconstruction analysis has an efficiency of a few percent, and that a precise measurement of the masses of $\tilde{\nu}$, $\tilde{\chi}_1^\pm$, $\tilde{\chi}_1^0$ can be performed. Both the Standard Model background and the backgrounds from other SUSY pair productions were studied in detail, and shown to be well below the expected signal for a value of the considered R_p coupling λ'_{211} taken at the present low-energy limit.

The trilepton signal from sneutrino production was then studied as a function of the model parameters under different model assumptions, and sensitivity over a significant part of the parameter space was found. Within the MSSM, the production of a 900 GeV sneutrino for $\lambda'_{211} > 0.05$, and of a 350 GeV sneutrino for $\lambda'_{211} > 0.01$ can be observed in the first three years of LHC running. In the framework of the mSUGRA model, the region in the $m_0 - m_{1/2}$ space accessible to the analysis was mapped as a function of the value of the R_p -violating coupling for representative values of $\tan\beta$. A significant part of the $m_0 - m_{1/2}$ plane will be accessible for $\lambda'_{211} > 0.01$.

Although the detailed study was focused on the case of a single dominant

λ'_{211} coupling, we have found that the resonant sneutrino production analysis can bring interesting sensitivities on all the \mathcal{R}_p couplings of the type λ'_{2jk} , compared to the low-energy constraints. The resonant sneutrino production should also allow to test most of the λ'_{1jk} coupling constants.

In conclusion we have demonstrated that if minimal supersymmetry with R-parity violation is realised in nature, the three-leptons signature from sneutrino decay will be a privileged channel for the precision measurement of sparticle masses and for studying the SUSY parameter space, over a broad spectrum of models. Analyses based on the study of events including three leptons, were often advocated in the literature [33]-[46] as a particularly sensitive way of attacking the search for SUSY at the LHC in the standard R-conserving scenario. The higher lepton multiplicity and the possibility to perform precise measurements of the model parameters make this kind of analyses an even more attractive possibility in the case of R-parity violation with dominant λ' couplings.

Acknowledgements

This work was initiated during a workshop held in Les Houches. We warmly thank Patrick Aurenche and all of the organising team for the stimulating program, the excellent atmosphere and the outstanding computing facilities. We are also deeply indebted to the HERWIG team for allowing us to use a prerelease of the HERWIG 6.0 MonteCarlo.

References

- [1] H. Dreiner, published in *Perspectives on Supersymmetry*, ed. by G.L. Kane, World Scientific (1998), hep-ph/9707435.
- [2] S. Dimopoulos and L.J. Hall, Phys. Lett. **B 207**, 210 (1987).
- [3] H. Dreiner and G. G. Ross, Nucl. Phys. **B 365**, 597 (1991).
- [4] V. Barger, G. F. Giudice and T. Han, Phys. Rev. **D 40**, 2987 (1989).
- [5] G. Bhattacharyya, Invited talk presented at ‘Beyond the Desert’, Castle Ringberg, Tegernsee, Germany, 8-14 June 1997; Susy ’96, Nucl. Phys. B (Proc. Suppl.) **52A** 83 (1997).
- [6] R. Barbier et al., Report of the Group on the R-parity Violation, hep-ph/9810232.

- [7] F. Ledroit and G. Sajot, GDR-S-008 (ISN, Grenoble, 1998).
- [8] B. C. Allanach, A. Dedes, H. Dreiner, Phys. Rev. **D60**, 075014 (1999).
- [9] S. Dimopoulos, R. Esmailzadeh, L.J. Hall, J. Merlo and G.D. Starkman, Phys. Rev. **D41**, 2099 (1990).
- [10] P. Binetruy et al., ECFA Large Hadron Collider (LHC) Workshop, Aachen, 1990, Vol. II.
- [11] A. Datta, J. M. Yang, B.-L. Young and X. Zhang, Phys. Rev. **D56**, 3107 (1997).
- [12] R. J. Oakes, K. Whisnant, J. M. Yang, B.-L. Young and X. Zhang, Phys. Rev. **D57**, 534 (1998).
- [13] J. L. Hewett and T. G. Rizzo, “Proceedings of the XXIX International Conference on High Energy Physics”, Vancouver, CA, 23-29 July 1998, hep-ph/9809525.
- [14] P. Chiappetta et al., hep-ph/9910483.
- [15] J. Kalinowski, R. Rückl, H. Spiesberger and P. M. Zerwas, Phys. Lett. **B414**, 297 (1997).
- [16] J. Kalinowski, Proceedings of “*Beyond the Desert 97 – Accelerator and Non-Accelerator Approaches*”, Ringberg Castle, Germany, June 1997, hep-ph/9708490.
- [17] S. Bar-Shalom, G. Eilam and A. Soni, Phys. Rev. **D59**, 055012 (1999).
- [18] E. L. Berger, B. W. Harris and Z. Sullivan, Phys. Rev. Lett. **83**, 4472 (1999).
- [19] H. Dreiner, P. Richardson and M. H. Seymour, to appear in the proceedings of the BTMSSM subgroup of the Physics at Run II Workshop on Supersymmetry/Higgs, hep-ph/9903419.
- [20] H. Dreiner, P. Richardson and M. H. Seymour, hep-ph/0001224.
- [21] I. Hinchliffe and F. Paige, hep-ph/9907919.
- [22] SUSYGEN 3.0/06 N. Ghodbane, S. Katsanevas, P. Morawitz and E. Perez, lyoinfo.in2p3.fr/susygen/susygen3.html; N. Ghodbane, hep-ph/9909499.
- [23] JETSET 7.3 and 7.4; T. Sjöstrand, Lund Univ. preprint LU-TP-95-20 (August 1995) 321pp; *idem*, CERN preprint TH-7112-93 (February 1994) 305pp.

- [24] V.N. Gribov et L.N. Lipatov, Sov. Journ. Nucl. Phys. 15 (1972) 78;
G. Altarelli et G. Parisi, Nucl. Phys. B126 (1977) 298;
Y.L. Dokshitzer, JETP 46 (1977) 641.
- [25] E. Richter-Was, D. Froidevaux, L. Poggioli, 'ATLFAST 2.0: a fast simulation package for ATLAS', ATLAS Internal Note ATL-PHYS-98-131 (1998).
- [26] T. Sjöstrand, Comp. Phys. Comm. **82**, 74 (1994).
- [27] D.O. Carlson, S. Mrenna, C.P. Yuan, private communication;
D.O. Carlson and C.P. Yuan, Phys. Lett. **B306**, 386 (1993).
- [28] H. Baer, F.E. Paige, S.D. Protopopescu, and X. Tata, hep-ph/9305342;
ibid., hep-ph/9804321 (1998).
- [29] HERWIG 6.1 Release Note, hep-ph/9912396; G. Marchesini, B. R. Webber,
G. Abbiendi, I. G. Knowles, M. H. Seymour and L. Stanco, Computer Phys.
Commun. **67**, 465 (1992).
- [30] The ALEPH Collaboration, Internal Note ALEPH 99-078, CONF 99-050
(1999), contributed to HEP-EPS 99.
- [31] The ATLAS Collaboration, 'ATLAS Detector and Physics Performance
Technical Design Report', ATLAS TDR 15, CERN/LHCC/99-15 (1999).
- [32] G. Moreau et al., To appear in Phys. Lett. **B**, hep-ph/9910341.
- [33] P. Nath and R. Arnowitt, Mod. Phys. Lett. **A 2**, 331 (1987).
- [34] R. Arnowitt, R. Barnett, P. Nath and F. Paige, Int. J. Mod. Phys. **A 2**,
1113 (1987).
- [35] H. Baer, K. Hagiwara and X. Tata, Phys. Rev. **D35**, 1598 (1987).
- [36] R. Barbieri, F. Caravaglios, M. Frigeni and M. Mangano, Nucl. Phys. **B**
367, 28 (1991).
- [37] T. Kamon, J. L. Lopez, P. McIntyre, and J. T. White, Phys. Rev. **D50**,
5676 (1994).
- [38] H. Baer, C.-H. Chen, C. Kao and X. Tata, Phys. Rev. **D52**, 1565 (1995).
- [39] S. Mrenna, G. Kane, G. Kribs and J. Wells, Phys. Rev. **D53**, 1168 (1996).
- [40] H. Baer, C.-H. Chen, M. Drees, F. Paige and X. Tata, Phys. Rev. Lett. **79**,
986 (1997).
- [41] H. Baer, C.-H. Chen, M. Drees, F. Paige and X. Tata, Phys. Rev. **D58**,
075008 (1998).

- [42] V. Barger, C. Kao and T.-J. Li., Phys. Lett. **B433**, 328 (1998).
- [43] V. Barger and C. Kao, preprint FERMILAB-PUB-98/342-T, Phys. Rev. **D60**, 115015 (1999).
- [44] J. Lykken and K. T. Matchev, preprint FERMILAB-PUB-99/034-T, Phys. Rev. **D61**, 015001 (2000).
- [45] K. T. Matchev and D. M. Pierce, preprint FERMILAB-PUB-99/078-T, Phys. Rev. **D60**, 075004 (1999).
- [46] H. Baer, M. Drees, F. Paige, P. Quintana, X. Tata, hep-ph/9906233.